MAGNETOHYDRODYNAMIC FLOW OF NANOFLUID WITH HOMOGENEOUS-HETEROGENEOUS REACTIONS AND VELOCITY SLIP

by

Tasawar HAYAT [a,b], Maria IMTIAZ [a*], and Ahmad ALSAEDI [b]

[a] Department of Mathematics, Quaid-I-Azam University, Islamabad, Pakistan
[b] NAAM Research Group, Department of Mathematics, Faculty of Science, King Abdulaziz University, Jeddah, Saudi Arabia

Original scientific paper
https://doi.org/10.2998/TSCI140922067H

This article focuses on the steady magnetohydrodynamic flow of viscous nanofluid. The flow is caused by a stretching surface with homogeneous-heterogeneous reactions. An incompressible fluid fills the porous space. Copper-water and silver-water nanofluids are investigated in this study. Transformation method reduces the non-linear partial differential equations governing the flow into the ordinary differential equation by similarity transformations. The obtained equations are then solved for the development of series solutions. Convergence of the obtained series solutions is explicitly discussed. Effects of different parameters on the velocity, concentration and skin friction coefficient are shown and analyzed through graphs.

Keywords: *magnetohydrodynamic nanofluid, homogeneous-heterogeneous reactions, porous medium, velocity slip condition*

Introduction

The traditional heat transfer fluids like oil, water, and ethylene glycol mixtures are now recognized as the poor heat transfer fluids. Addition of solid nanoparticles in traditional heat transfer fluids enhances the thermal conductivity of base fluid. The term nanofluid is credited by Choi [1]. This pioneering experimental research witnessed thermal conductivity enhancement of a nanofluid. He concluded that addition of very small amount of nanoparticles to traditional heat transfer liquids enhanced the thermal conductivity of liquid up to two times. Eastman *et al*. [2] and Choi *et al*. [3] pointed out that a small amount (<1% volume fraction) of Cu nanoparticles or carbon nanotubes dispersed in ethylene glycol or oil remarkably enhanced the thermal conductivity of a fluid by 40% and 50%, respectively. Thus the nanomaterials are recognized more effective in micro/nano electromechanical devices, advanced cooling systems, large scale thermal management systems via evaporators, heat exchangers and industrial cooling applications. Such fluids are very stable with no extra issues of erosion, sedimentation, non-Newtonian properties and additional pressure drop. This is because of tiny size and low volume fraction of nano elements required for thermal conductivity enhancement. Further the canvas of magnetic field has important applications in medicine, physics and engineering. Many equipment such as MHD generators, pumps, bearings and boundary layer control are affected by the interaction between the electrically conducting fluid and a

* Corresponding author, email: mi_qau@yanoo.com

magnetic field. The behavior of the flow strongly depends on the orientation and intensity of the applied magnetic field. The exerted magnetic field manipulates the suspended particles and rearranges their concentration in the fluid which strongly changes heat transfer characteristics of the flow. A magnetic nanofluid has both the liquid and magnetic characteristics. Such material have fascinating applications like optical modulators, magneto-optical wavelength filters, non-linear optical materials, optical switches, optical gratings, *etc*. Magnetic particles have pivoted role in the construction of loud speakers as sealing materials and in sink float separation. Magneto nanofluids are useful to guide the particles up the blood stream to a tumor with magnets. This is due to the fact that the magnetic nanoparticles are regarded more adhesive to tumor cells than non-malignant cells. Such particles absorb more power than micro particles in alternating current magnetic fields tolerable in humans *i. e*. for cancer therapy. Numerous applications involving nanofluids include drug delivery, hyperthermia, constrast enhancement in magnetic resonance imaging and magnetic cell separation. Motivated by all the aforementioned facts, various scientists and engineers are engaged in the discussion of flows of nanofluids via different aspects (see [4-18] and many useful attempts therein).

Homogeneous-heterogeneous reactions occur in many chemically reacting systems such as in combustion, catalysis, and biochemical systems. The interaction between the homogeneous reactions in the bulk of the fluid and heterogeneous reactions occurring on some catalytic surfaces is generally complex and is involved in the production and consumption of reactant species at different rates both within the fluid and on the catalytic surfaces. A model for isothermal homogeneous-heterogeneous reactions in boundary layer flow of viscous fluid past a flat plate is studied by Merkin [19]. He presented the homogeneous reaction by cubic autocatalysis and the heterogeneous reaction by a first order process and showed that the surface reaction is the dominant mechanism near the leading edge of the plate. Chaudhary and Merkin [20] studied the homogenous-heterogeneous reactions in boundary layer flow of viscous fluid. They found the numerical solution near the leading edge of a flat plate. Bachok *et al*. [21] focused on the stagnation-point flow towards a stretching sheet with homogeneous--heterogeneous reactions effects. Effects of homogeneous-heterogeneous reactions on the flow of viscoelastic fluid towards a stretching sheet are investigated by Khan and Pop [22]. Kameswaran *et al*. [23] extended the work of [22] for nanofluid over a porous stretching sheet.

In general, porous medium is used for transport and storage of energy. Analysis of flow through a porous medium has become the core of several scientific and engineering applications. These applications include the utilization of geothermal energy, the migration of moisture in fibrous insulation, food processing, casting and welding in manufacturing processes, the dispersion of chemical contaminants in different industrial processes, the design of nuclear reactors, chemical catalytic reactors, compact heat exchangers, solar power, and many others. Further the use of micro/nano electromechanical systems (MEMS/NEMS) has been increased in many industries. Such systems have association with velocity slip [24-28].

Motivated by such facts, the main concern in present communication is to examine the flow analysis of nanofluid with homogeneous-heterogeneous reactions and velocity slip. The relevant problems for velocity and concentration are modeled. The non-linear partial differential equations are converted into the ordinary differential equations. Resulting equations are computed for the series solutions by a modern technique namely the homotopy analysis method (HAM) [29-33]. Convergence region of the derived solutions is determined. Discussion relevant to embedded parameters is made using graphical illustration.

Model development

Let us consider the steady 2-D flow of an incompressible nanofluid over a stretching surface in porous medium with permeability *K*. The x-axis is taken along the stretching surface in the direction of motion and y-axis is perpendicular to it. A uniform transverse magnetic field of strength, B_0, is applied parallel to the y-axis. It is assumed that the induced magnetic and electric fields effects are negligible, fig. 1. Nanoparticles such as Cu and Ag are considered. Water is treated as a base fluid.

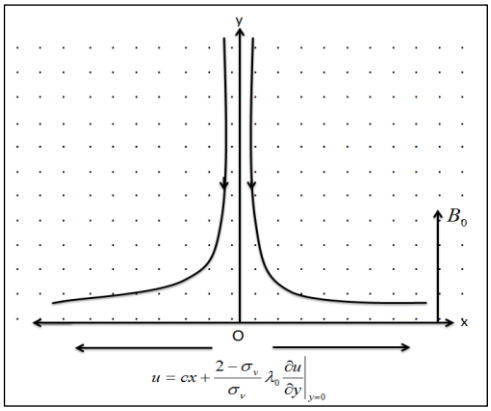

Figure 1. Geometry of the problem

We have taken a simple homogeneous--heterogeneous reaction model in the following form [16]:

$$A + 2B \rightarrow 3B, \quad \text{rate} = k_c ab^2 \tag{1}$$

while on the catalyst surface we have the single, isothermal, first order reaction

$$A \rightarrow B, \quad \text{rate} = k_s a \tag{2}$$

where a and b are the concentrations of the chemical species A and B and k_c and k_s denote the rate constants. We assume that both reaction processes are isothermal. Under these assumptions, the relevant boundary layer equations are:

$$\frac{\partial u}{\partial x} + \frac{\partial v}{\partial y} = 0 \tag{3}$$

$$\rho_{\text{nf}}\left(u\frac{\partial u}{\partial x} + v\frac{\partial u}{\partial y}\right) = \mu_{\text{nf}}\frac{\partial^2 u}{\partial y^2} - \frac{\mu_{\text{nf}}}{K}u - \sigma B_0^2 u \tag{4}$$

$$u\frac{\partial a}{\partial x} + v\frac{\partial a}{\partial y} = D_A\frac{\partial^2 a}{\partial y^2} - k_c ab^2 \tag{5}$$

$$u\frac{\partial b}{\partial x} + v\frac{\partial b}{\partial y} = D_B\frac{\partial^2 b}{\partial y^2} + k_c ab^2 \tag{6}$$

The subjected boundary conditions are:

$$u = cx + \frac{2-\sigma_v}{\sigma_v}\lambda_0\frac{\partial u}{\partial y}\Big|_{y=0}, \quad v = 0,\ D_A\frac{\partial a}{\partial y} = k_s a, \quad D_B\frac{\partial b}{\partial y} = -k_s a \ \text{ at } y = 0,$$
$$u \rightarrow 0,\ a \rightarrow a_0,\ b \rightarrow 0 \ \text{ as } y \rightarrow \infty \tag{7}$$

where u and v are the velocity components along the x- and y-directions, respectively, D_A and D_B are the respective diffusion species coefficients of A and B, σ is the electrical conductivity of fluid, σ_v – the tangential momentum accommodation coefficient, and λ_0 – the molecular mean free path. The effective density, ρ_{nf}, the dynamic viscosity, μ_{nf}, the heat capacitance, $(\rho c_p)_{\text{nf}}$, and the thermal conductivity, k_{nf}, of the nanofluid are given by:

$$\rho_{\mathrm{nf}} = \rho_{\mathrm{f}}(1-\varphi) + \rho_{\mathrm{s}}\varphi \tag{8}$$

$$\mu_{\mathrm{nf}} = \frac{\mu_{\mathrm{f}}}{(1-\varphi)^{2.5}} \tag{9}$$

$$(\rho c_p)_{\mathrm{nf}} = (\rho c_p)_{\mathrm{f}}(1-\varphi) + (\rho c_p)_{\mathrm{s}}\varphi \tag{10}$$

$$\frac{k_{\mathrm{nf}}}{k_{\mathrm{f}}} = \frac{k_s + 2k_{\mathrm{f}} - 2\varphi(k_{\mathrm{f}} - k_s)}{k_s + 2k_{\mathrm{f}} + 2\varphi(k_{\mathrm{f}} - k_s)} \tag{11}$$

Here ϕ is the nanoparticle volume fraction, s in subscript is for nanosolid-particles and f in subscript is for base fluid. Denoting a_0 (a constant) and $g(\eta)$ and $h(\eta)$ the dimensionless concentration and defining:

$$\eta = \sqrt{\frac{c}{\nu_{\mathrm{f}}}}y, \quad u = cxf'(\eta), \quad v = -\sqrt{c\nu_{\mathrm{f}}}\, f(\eta), \quad a = a_0 g(\eta), \quad b = a_0 h(\eta) \tag{12}$$

Equation (3) is satisfied automatically and eqs. (4)-(7) reduce to:

$$f''' + \varphi_1(ff'' - f'^2) - \lambda f' - (1-\varphi)^{2.5}\mathrm{Ha}f' = 0 \tag{13}$$

$$\frac{1}{\mathrm{Sc}}g'' + fg' - kgh^2 = 0 \tag{14}$$

$$\frac{\delta}{\mathrm{Sc}}h'' + fh' + kgh^2 = 0 \tag{15}$$

$$f'(0) = 1 + \gamma f''(0), \quad f(0) = 0, \quad f'(\infty) \to 0 \tag{16}$$

$$g'(0) = K_s g(0), \quad g(\infty) \to 1 \tag{17}$$

$$\delta h'(0) = -K_s g(0), \quad h(\infty) \to 0 \tag{18}$$

in which prime indicates the differentiation with respect to η. Moreover the non-dimensional constants in eqs. (13)-(18) are the porosity parameter, λ, the Hartman number, the Schmidt number, the measure of the strength of the homogeneous reaction, k, the measure of the strength of the heterogeneous reaction, K_s, the ratio of the diffusion coefficient, δ, and the velocity slip parameter, γ. These are defined:

$$\lambda = \frac{\nu_{\mathrm{f}}}{cK}, \ \mathrm{Ha} = \frac{\sigma B_0^2}{c\rho_{\mathrm{f}}}, \ \mathrm{Sc} = \frac{\nu_{\mathrm{f}}}{D_A}, \ k = \frac{k_c a_0^2}{c}, \ K_s = \frac{k_s}{D_A}\sqrt{\frac{\nu_{\mathrm{f}}}{c}}, \ \delta = \frac{D_B}{D_A}, \ \gamma = \frac{2-\sigma_v}{\sigma_v}\lambda_0\sqrt{\frac{c}{\nu_{\mathrm{f}}}} \tag{19}$$

where

$$\varphi_1 = (1-\varphi)^{2.5}\left(1 - \varphi + \varphi\frac{\rho_s}{\rho_f}\right) \tag{20}$$

The diffusion coefficients of chemical species A and B are expected to be of a comparable size. This leads to make a further assumption that the diffusion coefficients D_A and D_B are equal, *i. e*. to take $\delta = 1$ [16]. In this case we have from eqs. (17) and (18):

$$g(\eta)+h(\eta)=1 \tag{21}$$

Thus eqs. (14) and (15) become:

$$\frac{1}{\mathrm{Sc}}g''+fg'-kg(1-g)^2=0 \tag{22}$$

subject to the boundary conditions:

$$g'(0)=K_s g(0), \qquad g(\infty)\to 1 \tag{23}$$

The physical quantity of interest is the skin-friction coefficient, C_f. It characterizes the surface drag. The shearing stress at the surface of the wall, τ_w, is given by:

$$\tau_w=-\mu_{\mathrm{nf}}\left.\frac{\partial u}{\partial y}\right|_{y=0}=-\frac{1}{(1-\varphi)^{2.5}}\sqrt{\mu_\mathrm{f}\rho_\mathrm{f}c^3}\,xf''(0) \tag{24}$$

The skin friction coefficient is defined:

$$C_f=\frac{\tau_w}{0.5\rho_\mathrm{f}u_w^2} \tag{25}$$

$$C_f\sqrt{\mathrm{Re}_x}=-\frac{2}{(1-\varphi)^{2.5}}f''(0) \tag{26}$$

in which $\mathrm{Re}_x=u_w x/\nu_\mathrm{f}$ denotes the local Reynolds number.

Solutions derivation

Zeroth-order deformation problems

We choose the initial guesses $f_0(\eta)$ and $g_0(\eta)$ and the linear operators $\mathbf{L}_f$ and $\mathbf{L}_g$ in the forms:

$$f_0(\eta)=\frac{1}{1+\gamma}[1-\mathrm{e}^{-\eta}], \qquad g_0(\eta)=1-\frac{1}{2}\mathrm{e}^{-K_s\eta} \tag{27}$$

$$\mathbf{L}_f(f)=f'''-f', \qquad \mathbf{L}_g(g)=g''-g \tag{28}$$

together with the properties:

$$\mathbf{L}_f\left[c_1+c_2\mathrm{e}^{\eta}+c_3\mathrm{e}^{-\eta}\right]=0, \qquad \mathbf{L}_g\left[c_4\mathrm{e}^{\eta}+c_5\mathrm{e}^{-\eta}\right]=0 \tag{29}$$

where c_1-c_5 are constants. With eqs. (13) and (22), the definitions of operators $\mathbf{N}_f$ and $\mathbf{N}_g$ are:

$$\mathbf{N}_f\left[\hat f(\eta,p),\hat g(\eta,p)\right]=\frac{\partial^3\hat f(\eta,p)}{\partial\eta^3}+\varphi_1\left[\hat f(\eta,p)\frac{\partial^2\hat f(\eta,p)}{\partial\eta^2}-\left(\frac{\partial\hat f(\eta,p)}{\partial\eta}\right)^2\right]-$$
$$-\lambda\frac{\partial\hat f(\eta,p)}{\partial\eta}-(1-\varphi)^{2.5}\mathrm{Ha}\frac{\partial\hat f(\eta,p)}{\partial\eta} \tag{30}$$

$$\mathbf{N}_g[\hat{g}(\eta,p),\hat{f}(\eta,p)]=$$
$$=\frac{1}{\mathrm{Sc}}\frac{\partial^2\hat{g}(\eta,p)}{\partial\eta^2}+\hat{f}(\eta,p)\frac{\partial\hat{g}(\eta,p)}{\partial\eta}-k\hat{g}(\eta,p)-k[\hat{g}(\eta,p)]^3+2k[\hat{g}(\eta,p)]^2 \tag{31}$$

We construct the zeroth order problems:

$$(1-p)\mathbf{L}_f[\hat{f}(\eta,p)-f_0(\eta)]=p\hbar_f\mathbf{N}_f[\hat{f}(\eta,p)] \tag{32}$$

$$(1-p)\mathbf{L}_g[\hat{g}(\eta,p)-g_0(\eta)]=p\hbar_g\mathbf{N}_g[\hat{g}(\eta,p)] \tag{33}$$

$$\hat{f}'(0,p)=1+\gamma\hat{f}''(0,p),\quad \hat{f}(0,p)=0,\quad \hat{f}'(\infty,p)=0,\quad \hat{g}'(0,p)=K_s\hat{g}(0,p),\quad \hat{g}(\infty,p)=1 \tag{34}$$

where $\hbar_f$ and $\hbar_g$ are the non-zero auxiliary parameters and for $p = 0$ and $p = 1$ we have:

$$\hat{f}(\eta,0)=f_0(\eta),\quad \hat{f}(\eta,1)=f(\eta),\quad \hat{g}(\eta,0)=g_0(\eta),\quad \hat{g}(\eta,1)=g(\eta) \tag{35}$$

Note that $f_0(\eta)$ and $g_0(\eta)$ approach $f(\eta)$ and, $g(\eta)$, respectively, when p has variation from 0 to1. According to Taylor series we have:

$$\begin{aligned}\hat{f}(\eta,p)&=f_0(\eta)+\sum_{m=1}^{\infty}f_m(\eta)p^m,\ f_m(\eta)=\frac{1}{m!}\frac{\partial^m\hat{f}(\eta,p)}{\partial p^m}\bigg|_{p=0}\\ \hat{g}(\eta,p)&=g_0(\eta)+\sum_{m=1}^{\infty}g_m(\eta)p^m,\ g_m(\eta)=\frac{1}{m!}\frac{\partial^m\hat{g}(\eta,p)}{\partial p^m}\bigg|_{p=0}\end{aligned} \tag{36}$$

where the convergence depends upon $\hbar_f$ and $\hbar_g$. By proper choice of $\hbar_f$ and $\hbar_g$ the series (36) converge for $p = 1$ and so:

$$f(\eta)=f_0(\eta)+\sum_{m=1}^{\infty}f_m(\eta),\qquad g(\eta)=g_0(\eta)+\sum_{m=1}^{\infty}g_m(\eta) \tag{37}$$

The m^{th} order deformation problems

The resulting problems at this order are given by:

$$\mathbf{L}_f\left[f_m(\eta,p)-\chi_m f_{m-1}(\eta)\right]=\hbar_f\mathbf{R}_{f,m}(\eta) \tag{38}$$

$$\mathbf{L}_g\left[g_m(\eta,p)-\chi_m g_{m-1}(\eta)\right]=\hbar_g\mathbf{R}_{g,m}(\eta) \tag{39}$$

$$f_m(0)=f_m'(0)-\gamma f_m''(0)=f_m'(\infty)=g_m'(0)-K_s g_m(0)=g_m(\infty)=0 \tag{40}$$

$$\chi_m=\begin{cases}0, & m\le 1\\ 1, & m>1\end{cases} \tag{41}$$

$$\mathbf{R}_{f,m}(\eta)=f_{m-1}'''+\varphi_1\sum_{l=0}^{m-1}[f_{m-1-l}f_l''-f_{m-1-l}'f_l']-\lambda f_{m-1}'-(1-\varphi)^{2.5}\mathrm{Ha}f_{m-1}' \tag{42}$$

$$\mathbf{R}_{g,m}(\eta) = \frac{1}{\mathrm{Sc}} g''_{m-1} + \sum_{l=0}^{m-1} [g'_{m-1-l} f_l - k g_{m-1-l} \sum_{j=0}^{l} g_{l-j} g_j + 2k g_{m-1-l} g_l] - k g_{m-1} \tag{43}$$

where the general solutions are:

$$f_m(\eta) = f_m^*(\eta) + c_1 + c_2 \mathrm{e}^{\eta} + c_3 \mathrm{e}^{-\eta}, \quad g_m(\eta) = g_m^*(\eta) + c_4 \mathrm{e}^{\eta} + c_5 \mathrm{e}^{-\eta} \tag{44}$$

in which f_m^* and g_m^* denote the special solutions.

Analysis of the results

Convergence of the derived series solutions

Now the solutions of eqs. (13) and (22) subject to the boundary conditions (16) and (23) are computed by means of HAM. We choose auxiliary parameters $\hbar_f$ and $\hbar_g$ for the functions *f* and *g*, respectively. The convergence of obtained series and rate of the approximation for HAM strongly depend upon the values of the auxiliary parameters. For ranges of admissible values of $\hbar_f$ and $\hbar_g$, the $\hbar$-curves for 13$^{\text{th}}$-order of approximations are plotted in figs. 2 and 5. We can see that the permissible values for $\hbar_f$ and $\hbar_g$ for Cu-water are $-1.6 \le \hbar_f \le -0.5$ and $-1.2 \le \hbar_g \le -0.3$ and for Ag-water are $-1.6 \le \hbar_f \le -0.6$ and $-1 \le \hbar_g \le -0.1$ Further, the series solutions converge in the whole region of η $(0 < \eta < \infty)$ when $\hbar_f = \hbar_g = -1$.

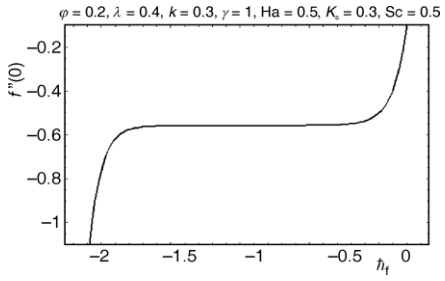

Figure 2. The $\hbar$- curve of f for Cu-water

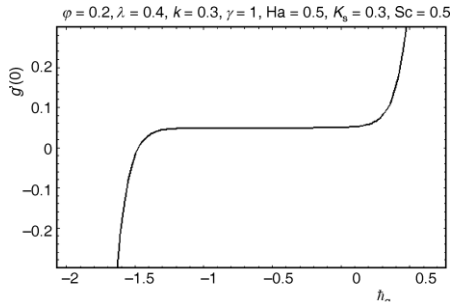

Figure 3. The $\hbar$- curve of g for Cu-water

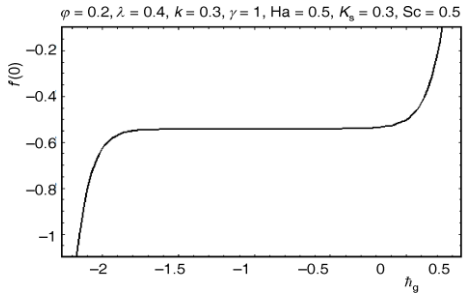

Figure 4. The $\hbar$- curve of f for Ag-water

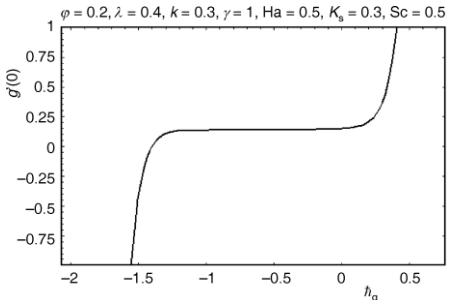

Figure 5. The $\hbar$- curve of g for Ag-water

Table 1 shows the convergence of the series solutions. It is observed that convergence is achieved at 17$^{\text{th}}$ order of approximations. In tab. 2 some existing thermophysical properties of water and nanoparticles are given.

Table 1. Convergence of HAM solutions for different order of approximations when φ = 0.2, λ = 0.4, k = 0.3, γ = 1, Ha = 0.5, K_s = 0.3, and Sc = 0.5

Order of approximations	$-f''(0)$	$g'(0)$
1	0.5455	0.04916
5	0.5564	0.04835
10	0.5588	0.04788
15	0.5596	0.04741
17	0.5594	0.04736
20	0.5594	0.04736
25	0.5594	0.04736

Table 2. Thermophysical properties of water and nanoparticles

	$\rho(kg/m^3)$	$c_p(j/kgk)$	$k(W/mk)$	$\beta\cdot10^5(K^{-1})$
Pure water	997.1	4179	0.613	21
Copper, Cu	8933	385	401	1.67
Silver, Ag	10500	235	429	1.89
Alumina, Al_2O_3	3970	765	40	0.85
Titanium Oxide, TiO_2	4250	686.2	8.9538	0.9

Results and discussion

The effects of different parameters on the dimensionless flow and concentration profiles are investigated and presented graphically in this section.

Dimensionless velocity profiles

Figures 6-9 exhibit the dimensionless velocity profiles for different values of nanoparticle volume fraction, φ, Hartman number, velocity slip parameter, γ, and porosity parameter, λ. Effects of volume fraction of nanoparticles Cu and Ag on the velocity profile f' can be seen from fig. 6. Here the velocity profile and boundary layer thickness decrease when volume fraction for the nanoparticles increases. The effects of Hartman number on the velocity f' are depicted in fig. 7. We analyzed that the velocity is reduced when we increase the values of Hartman number. In fact applied magnetic field has the tendency to slow down the movement of the fluid which leads to a decrease in the velocity and momentum boundary layer thickness. Variations of velocity slip parameter γ on velocity profile f' can be seen in fig. 8. There is a decrease in velocity when velocity slip parameter γ is increased. From fig. 9, we have seen that larger values of porosity parameter λ correspond to the less velocity. Porosity parameter depends on the permeability parameter K Increase in porosity parameter leads to the lower permeability parameter. This lower permeability parameter causes a reduction in the fluid velocity.

Dimensionless concentration profiles

Effects of the measure of the strength of the homogeneous reaction, k, the measure of the strength of the heterogeneous reaction, K_s, and the Schmidt number on the concentration profile, g, are shown in figs.10-12. Effects of k on the concentration are analyzed in fig. 10. It is observed that increasing the measure of the strength of the homogeneous reaction k

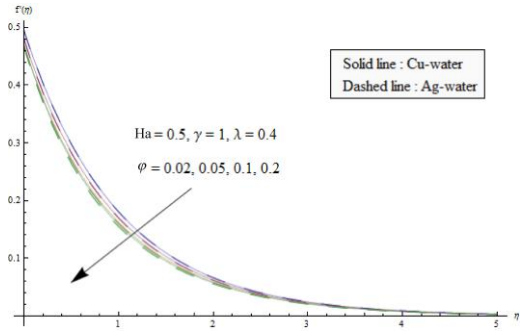

Figure 6. Effects of φ on f'

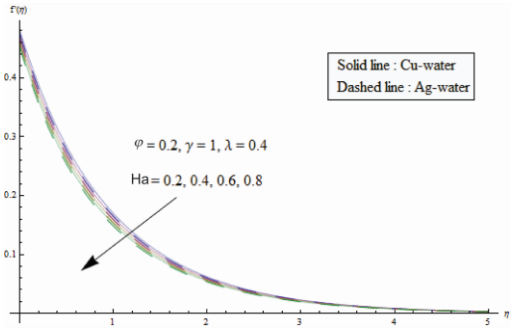

Figure 7. Effects of Ha on f'

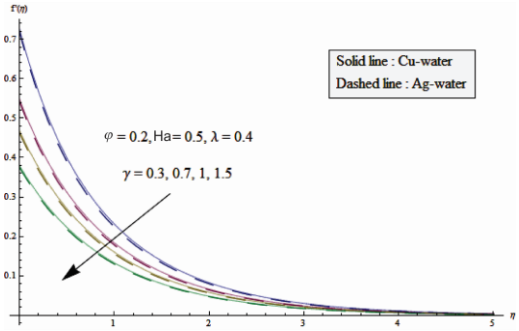

Figure 8. Effects of γ on f'

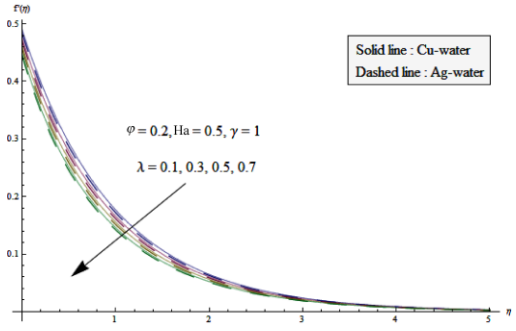

Figure 9. Effects of λ on f'

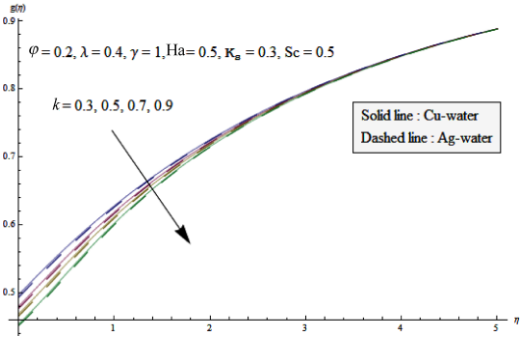

Figure 10. Effects of k on g

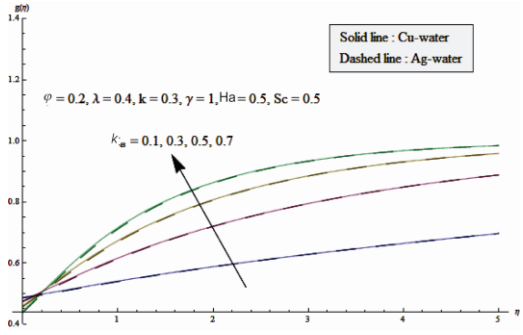

Figure 11. Effects of K_s on g

decreases the thermal boundary layer thickness. Figure 11 illustrates the effects of K_s on concentration profile g. There is an increase in concentration g when the measure of the strength of the heterogeneous reaction K_s is increased. The behavior of Schmidt number on the concentration profile is similar to that of K_s (see fig.12).

Skin friction coefficient and concentration

Figure 13 shows the skin friction coefficient $f''(0)$ as a function of nanoparticle volume fraction φ. The skin friction coefficient enhances with increasing values of φ.

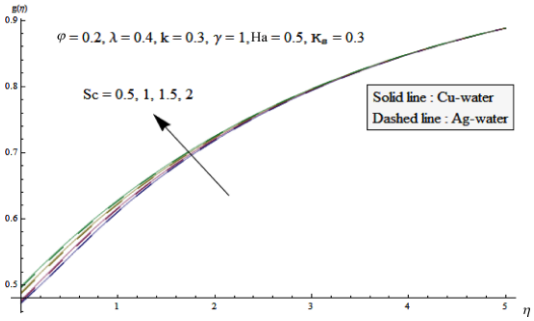

Figure 12. Effects of Sc on *g*

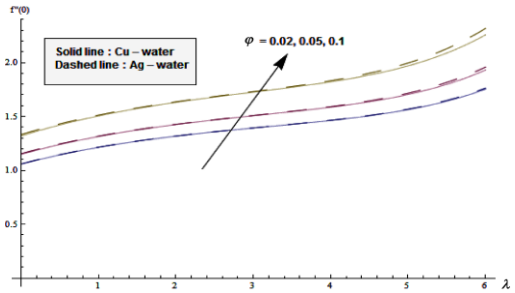

Figure 13. Effects of φ on skin friction coefficient

The results of the skin friction coefficient are examined for both types of nanofluids. We observe that the Ag-water nanofluid gives a higher drag force opposite to the flow when compared with the Cu-water nanofluid.

The variation of dimensionless concentration for different values of K_s and k are shown in figs. 14 and 15, respectively. From fig. 14 it is observed that concentration at the surface decreases as the strength of the heterogeneous reaction increases for different types of nanofluids. One can see from fig. 15 that $g(0)$ decreases with the increase of homogeneous reaction strength k. Influence of Sc on $g(0)$ for two different types of nanoparticles is shown in fig. 16. It is clear that the concentration decreases with an increase of Schmidt number. In tab. 3 some numerical values of skin friction coefficient are given for Cu and Ag nanoparticles. Tabular values show that skin friction coefficient increases by increasing φ and Ha while it decreases for larger γ. Table 4 shows that dimensionless concentration decreases by increasing K_s, Sc, k, and γ.

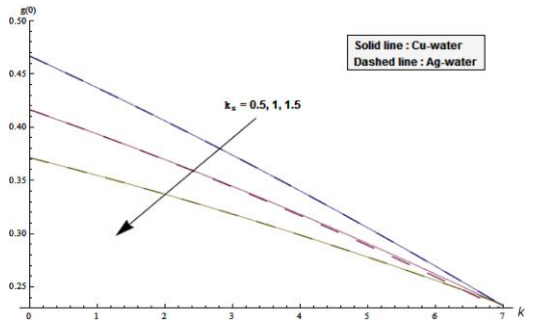

Figure 14. Effects of K_s on the concentration

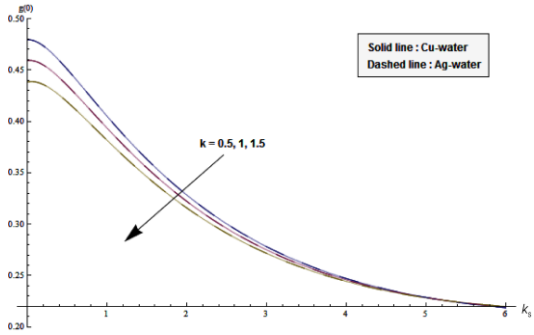

Figure 15. Effects of k on the concentration

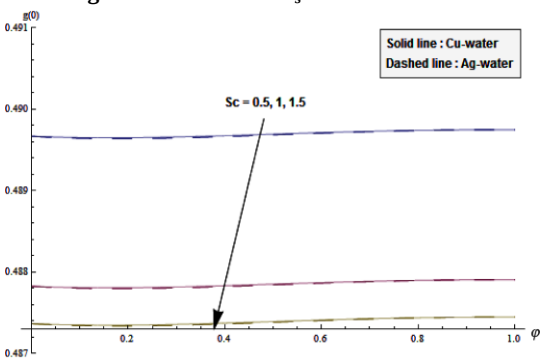

Figure 16. Effects of Sc on the concentration

Table 3. Numerical values of skin friction coefficient for Cu and Ag when $\lambda = 0.4$, $k = 0.3$, $K_s = 0.3$, and Sc =0.5

φ	Ha	γ	$C_f\sqrt{\mathrm{Re}_x}$ for Cu	$C_f\sqrt{\mathrm{Re}_x}$ for Ag
0.05	0.5	1.0	1.278	1.284
0.1			1.465	1.475
0.2			1.955	1.973
0.2	0.1		1.897	1.917
	0.3		1.928	1.945
	0.7		1.981	1.996
	0.5	0.1	4.542	4.672
		0.5	2.827	2.865
		0.9	2.079	2.098

Table 4. Numerical values of dimensionless concentration for Cu and Ag approximations when $\varphi = 0.2$, $\lambda = 0.4$, and Ha = 0.5

K_s	Sc	k	γ	$g(0)$ for Cu	$g(0)$ for Ag
0.5	0.5	0.3	1.0	0.4169	0.4173
1.0				0.3274	0.3321
1.5				0.2856	0.2741
0.5	0.4			0.4726	0.4675
	0.7			0. 4703	0.4561
	1.0			0.4675	0.4532
	0.5	0.5		0.4407	0.4413
		1.0		0.4087	0.3997
		1.5		0.3645	0.3761
		0.3	0.1	0.4618	0.4619
			0.5	0.4583	0.4537
			0.9	0.4565	0.4502

Concluding remarks

Here MHD flow of nanofluid by a stretching sheet in presence of homogeneous--heterogeneous reactions is considered. Convergent approximate solution is constructed. The following observations are made.

- An increase in the values of φ, Ha, γ, and λ has similar effects on the velocity $f'(\eta)$ in a qualitative sense.
- Concentration profile increases by increasing K_s and Sc while it decreases when k is increased.
- The values of skin friction coefficient are higher for Ag-water when φ enhances.
- Higher values of K_s, k, and Sc correspond to smaller values of dimensionless concentration.

Nomenclature

a – concentration of chemical specie A, [–]
B_0 – uniform magnetic field strength, [kgs A]
b – concentration of chemical specie B, [–]
C_f – local skin friction coefficient
c – stretching constant, [s]
c_p – specific heat, [m^2s^{-1}]
D_A – diffusion coefficient of specie A, [m^2s^{-1}]
D_B – diffusion coefficient of specie B, [m^2s^{-1}]
K – permeability, [m^2]
Ks – measure of the strength of the heterogeneous reaction, [–]

k – measure of the strength of the homogeneous reaction, [–]
k_c – homogeneous rate constant, [s^{-1}]
k_s – heterogeneous rate constant, [ms^{-1}]
$\mathbf{L}_f, \mathbf{L}_g$ – linear operator for velocity and concentration fields, [–]
Ha – Hartman number, [–]
$\mathbf{N}_f, \mathbf{N}_g$ – non-linear operators [–]
$\mathbf{R}_{f,m}$ $\mathbf{R}_{g,m}$ – m^{th} order non-linear operators [–]
Re_x – local Reynolds number
Sc – Schmidt number [–]
u, v – velocity components along x and y axes, respectively [ms^{-1}]
$\hbar_f, \hbar_g$ – non-zero auxiliary parameters, [–]

Greek symbols

γ – velocity slip parameter, [–]
δ – ratio of the diffusion coefficient, [–]
λ – porosity parameter, [–]
λ_0 – molecular mean free path, [m]
μ – viscosity, [$kgm^{-2}s^{-1}$]
ν – kinematic viscosity, [m^2s^{-1}]
ρ – density, [kgm^{-3}]
σ – electrical conductivity, [$s^3A^2kg^{-1}m^{-3}$]
σ_v – tangential momentum accommodation coefficient, [–]
τ_w – surface shear stress, [$kgs^{-1}m^{-3}$]
φ – nanoparticle volume fraction, [–]

Subscripts

f – base fluid
nf – nanofluid
s – nanosolid-particles

Superscripts

` – derivative with respective to η

Reference

[1] Choi, S. U. S., Enhancing Thermal Conductivity of Fluids with Nanoparticle, Proceedings, ASME International Mechanical Engineering Congress and Exposition, *66* (1995), Jan., pp. 99-105
[2] Eastman, J. A., *et al*., Anomalously Increased Effective Thermal Conductivity of Ethylene Glycol-Based Nanofluids Containing Copper Nanoparticles, *Applied Physics Letters, 78* (2001), 6, pp. 718-720
[3] Choi, S. U. S., *et al*., Anomalous Thermal Conductivities Enhancement on Nanotube Suspension, *Applied Physics Letters, 79* (2001), 14, pp. 2252-2254
[4] Turkyilmazoglu, M., Nanofluid Flow and Heat Transfer Due to a Rotating Disk, *Computers & Fluids, 94* (2014), May, pp. 139-146
[5] Turkyilmazoglu, M., Unsteady Convection Flow of Some Nanofluids Past a Moving Vertical Flat Plate with Heat Transfer, *Journal of Heat Transfer, 136* (2013), 3, 031704
[6] Sheikholeslami, M., Goriji-Bandpy, M., Free Convection of Ferrofluid in a Cavity Heated from Below in the Presence of an External Magnetic Field, *Powder Technology, 256* (2014), Apr., pp. 490-498
[7] Sheikholeslami, M., *et al*., Analytical Investigation of MHD Nanofluid Flow in a Semi-Porous Channel, *Powder Technology*, 246 (2013), Sept., pp. 327-336.
[8] Sheikholeslami, M., *et al*., Lattice Boltzmann Method for MHD Natural Convection Heat Transfer Using Nanofluid, *Powder Technology, 254* (2014), Mar., pp. 82-93
[9] Xu, H., *et al*., Flow and Heat Transfer in a Nano-Liquid Film Over an Unsteady Stretching Surface, *International Journal of Heat and Mass Transfer, 60* (2013), May, pp. 646-652
[10] Rashidi, M. M., *et al*., Entropy Generation in Steady MHD Flow Due to a Rotating Porous Disk in a Nanofluid, *International Journal of Heat and Mass Transfer, 62* (2013), Jul., pp. 515-525
[11] Niu, J., *et al*., Slip-Flow and Heat Transfer of a Non-Newtonian Nanofluid in a Microtube, *Plos One, 7* (2012), 5, e37274
[12] Khan, J. A., *et al*., On Model for Three-Dimensional Flow of Nanofluid: An Application to Solar Energy, *Journal of Molecular Liquids, 194* (2014), Jun., pp. 41-47
[13] Farooq, U., *et al*., Heat and Mass Transfer of Two-Layer Flows of Third-Grade Nanofluids in a Vertical Channel, *Applied Mathematics and Computation, 242* (2014), Sept., pp. 528-540
[14] Sheikholeslami, M., *et al*., Magnetic Field Effects on Natural Convection Around a Horizontal Circular Cylinder Inside a Square Enclosure Filled with Nanofluid, *International Communications in Heat and Mass Transfer, 39* (2012), 7, pp. 978-986
[15] Nadeem, S., et al., Heat Transfer Analysis of Water-Based Nanofluid Over an Exponentially Stretching Sheet, *Alexandria Engineering Journal, 53* (2014), 1, pp. 219-224
[16] Haq, R. U., *et al*., Thermophysical Effects of Carbon Nanotubes on MHD Flow over a Stretching Surface, *Physica E: Low-dimensional Systems and Nanostructures, 63* (2014), Sept., pp. 215-222
[17] Haq, R. U., *et al*., Convective Heat Transfer in MHD Slip Flow over a Stretching Surface in the Presence of Carbon Nanotubes, *Physica B: Condensed Matter, 457* (2015), 15, pp. 40-47

[18] Zhang, W. M., *et al*., A Review on Slip Models for Gas Microflows, *Journal of Microfluid Nanofluid, 13* (2012), 6, pp. 845-882
[19] Merkin, J. H., A Model for Isothermal Homogeneous-Heterogeneous Reactions in Boundary Layer Flow, *Mathematical and Computer Modelling, 24* (1996), 8, pp. 125-136
[20] Chaudhary, M. A., Merkin, J. H., A Simple Isothermal Model for Homogeneous-Heterogeneous Reactions in Boundary Layer Flow: I. Equal Diffusivities, *Fluid Dynamics Research, 16* (1995), 6, pp. 311-333
[21] Bachok, N., *et al*., On the Stagnation-Point Flow Towards a Stretching Sheet with Homogeneous-Heterogeneous Reactions Effects, *Communications in Nonlinear Science and Numerical Simulation, 16* (2011), 11, pp. 4296-4302
[22] Khan, W. A., Pop, I., Effects of Homogeneous-Heterogeneous Reactions on the Viscoelastic Fluid Towards a Stretching Sheet, *Journal of Heat Transfer, 134* (2012), 6, pp. 1-5
[23] Kameswaran, P. K., *et al*., Homogeneous-Heterogeneous Reactions in a Nanofluid Flow Due to Porous Stretching Sheet, *International Journal of Heat and Mass Transfer, 57* (2013), 2, pp. 465-472
[24] Rashidi, M. M., *et al*., Investigation of Entropy Generation in MHD and Slip Flow Over a Rotating Porous Disk with Variable Properties, *International Journal of Heat and Mass Transfer, 70* (2014), Mar., pp. 892-917
[25] Mahmoud, M. A. A., Waheed, S. E., MHD Flow and Heat Transfer of a Micropolar Fluid Over a Stretching Surface with Heat Generation (Absorption) and Slip Velocity, *Journal of the Egyptian Mathematical Society, 20* (2012), 1, pp. 20-27
[26] Ibrahim, W., Shankar, B., MHD Boundary Layer Flow and Heat Transfer of a Nanofluid Past a Permeable Stretching Sheet with Velocity, Thermal and Solutal Slip Boundary Conditions, *Computers & Fluids, 75* (2013), Apr., pp. 1-10
[27] Rooholghdos, S. A., Roohi, E., Extension of a Second Order Velocity Slip/Temperature Jump Boundary Condition to Simulate High Speed Micro/Nanoflows, *Computers & Mathematics with Applications, 67* (2014), 11, pp. 2029-2040
[28] Malvandi, A., Ganji, D. D., Brownian Motion and Thermophoresis Effects on Slip Flow of Alumina/Water Nanofluid Inside a Circular Microchannel in the Presence of a Magnetic Field, *International Journal of Thermal Sciences, 84* (2014), Oct., pp. 196-206
[29] Liao, S. J., On the Relationship Between the Homotopy Analysis Method and Euler Transform, *Communications in Nonlinear Science and Numerical Simulation, 15* (2010), 6, pp. 1421-1431
[30] Arqub, O. A., El-Ajou, A., Solution of the Fractional Epidemic Model by Homotopy Analysis Method, *Journal of King Saud University, 25* (2013), 1, pp. 73-81
[31] Turkyilmazoglu, M., A Note on Homotopy Analysis Method, *Applied Mathematics Letters, 23* (2010), 10, pp. 1226-1230
[32] Abbasbandy, S., Shivanian, E., Predictor Homotopy Analysis Method and its Application to Some Nonlinear Problems, *Comunications in Nonlinear Science and Numerical Simulation, 16* (2011), 6, pp. 2456-2468
[33] Shehzad S. A., *et al*., Thermophoresis Particle Deposition in Mixed Convection Three-Dimensional Radiative Flow of an Oldroyd-B Fluid, *Journal of Taiwan Institute of Chemical Engineers, 45* (2014), 3, pp. 787-794

Paper submitted: September 22, 2014
Paper revised: April 25, 2015
Paper accepted: April 25, 2015